Biophysical Journal Volume 68 May 1995 1814–1827

A Mutation in the Pore of the Sodium Channel Alters Gating

Gordon F. Tomaselli, Nipavan Chiamvimonvat, H. Bradley Nuss, Jeffrey R. Balser,*
Maria Teresa Pérez-García, Ruo Hui Xu, David W. Orias, Peter H. Backx, and Eduardo Marban
Department of Medicine, Division of Cardiology, and the *Department of Anesthesia and Critical Care Medicine, The Johns Hopkins School of Medicine, Baltimore, Maryland 21205 USA

ABSTRACT Ion permeation and channel gating are classically considered independent processes, but site-specific mutagenesis studies in K channels suggest that residues in or near the ion-selective pore of the channel can influence activation and inactivation. We describe a mutation in the pore of the skeletal muscle Na channel that alters gating. This mutation, *I*-W53C (residue 402 in the μ1 sequence), decreases the sensitivity to block by tetrodotoxin and increases the sensitivity to block by externally applied Cd^{2+} relative to the wild-type channel, placing this residue within the pore near the external mouth. Based on contemporary models of the structure of the channel, this residue is remote from the regions of the channel known to be involved in gating, yet this mutation abbreviates the time to peak and accelerates the decay of the macroscopic Na current. At the single-channel level we observe a shortening of the latency to first opening and a reduction in the mean open time compared with the wild-type channel. The acceleration of macroscopic current kinetics in the mutant channels can be simulated by changing only the activation and deactivation rate constants while constraining the microscopic inactivation rate constants to the values used to fit the wild-type currents. We conclude that the tryptophan at position 53 in the domain *I* P-loop may act as a linchpin in the pore that limits the opening transition rate. This effect could reflect an interaction of *I*-W53 with the activation voltage sensors or a more global gating-induced change in pore structure.

INTRODUCTION

Voltage-gated ion channels open in response to a change in transmembrane potential, exposing a pore through which ions cross the cell membrane. Classically, permeation and gating are considered to be independent processes (Hodgkin and Huxley, 1952). Nevertheless, several lines of evidence support a linkage between these two processes. Ions that permeate and/or block channels can influence gating in several ways. First, ions that block in the pore can slow channel closure by a foot-in-the-door mechanism (Armstrong, 1971). Second, permeant and blocking ions may modulate gating allosterically by occupying a gating site in the channel pore (Matteson and Swenson 1986; Miller et al., 1987; Demo and Yellen, 1992).

Evidence for structural coupling between permeation and gating has come from studies that combine the methods of electrophysiology and molecular genetics. Electrophysiological characterization of naturally occurring variants or mutant channels has produced several examples of primary structural changes that affect both permeation and gating in K channels. K^+ occupancy of an extracellular site near the pore has been shown to modulate the steady-state availability of several K channels (Pardo et al., 1992; Kirsch et al., 1992). Cytoplasmic domains that form part of the pore are also important in channel gating; conserved hydrophobic residues in the linker between the fourth and fifth membrane-spanning segments, thought to be part of the cytoplasmic vestibule of the channel, influence inactivation (McCormack et al., 1991; Isacoff et al., 1991). Indeed, it has been suggested that this region is part of a receptor for the inactivation ball (Hoshi et al., 1991; Isacoff et al., 1991). Binding of an NH_2-terminal ball to a cytoplasmic domain of the K channel is only one of several distinct types of inactivation gating (Hoshi et al., 1990; Hoshi et al. 1991), at least one of which involves the channel pore (Hoshi et al., 1991; De Biasi et al., 1993). Despite general structural homology between K channels and Na channels, interactions between gating and permeation are not well established in the Na channel.

The structural basis of fast inactivation in the Na channel involves a hydrophobic triplet of amino acid residues in the region linking the third and fourth internally homologous domains (Fig. 1) (Stühmer et al., 1989; West et al., 1992; Patton et al., 1992). This region of the Na channel is thought to form a lid that binds to a cytoplasmic region of the channel and occludes the pore. The structural basis of slower forms of Na channel inactivation is not as well described. Naturally occurring mutations outside the III-IV linker region can also affect the rate of current decay. Such mutations have been implicated in a group of neuromuscular diseases that afflict humans and horses, the adynamia-paramyotonia complex (for review see Rüdel et al., 1993). Activation is thought to involve movement of the highly charged fourth membrane-spanning segment (S4), although how translation of this segment produces channel opening is not defined. To date there are no clear examples of mutations in the Na channel pore that affect ion permeation and gating.

We report a mutation in the P-loop of the first domain of the skeletal muscle Na channel that simultaneously alters permeation and gating. Substitution of a cysteine for tryptophan in the first domain of the Na channel (*I*-W53C;

Received for publication 13 December 1994 and in final form 16 February 1995.

Address reprint requests to Dr. Gordon F. Tomaselli, Department of Medicine, Division of Cardiology, Johns Hopkins School of Medicine, Ross 844, 720 N. Rutland Ave., Baltimore, MD 21205. Tel.: 410-955-2774; Fax: 410-955-7953; E-mail: gtomasel@welchlink.welch.jhu.edu.

0006-3495/95/05/1814/14 $2.00

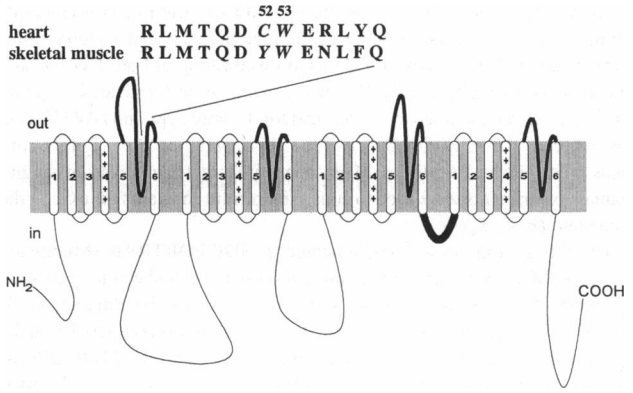

FIGURE 1 The predicted transmembrane topology of the voltage-dependent Na channel. Above the schematic, a portion of the sequence of the heart and skeletal muscle (μ1) channel P-loop is shown. The numbering scheme begins at the first conserved residue in the S5-S6 linker region (Tomaselli et al., 1993a). The italicized residues at position *I*-52 mediate the difference in Cd^{2+} and TTX sensitivity between the cardiac and skeletal muscle isoforms. The residue at *I*-53, a highly conserved tryptophan, is predicted to be further out of the pore of the channel.

Tomaselli et al., 1993a; see also Fig. 1) reduces the single-channel conductance and enhances the affinity for blockade by Cd^{2+} as compared with the wild-type channel, consistent with a location in the pore accessible from the extracellular solution. Remarkably, this substitution also accelerates activation and hastens whole-cell current decay. Single-channel recordings reveal that the *I*-W53C mutant exhibits substantial alterations of microscopic gating, including an abbreviated latency to first opening, reduced mean open times, and reduced open probability. Computer simulation of the experimental data indicates that the gating changes can be fully explained by mutation-induced changes in activation and deactivation rate constants. Preliminary reports have appeared (Tomaselli et al., 1993b,c).

MATERIALS AND METHODS

Mutagenesis and channel expression

Site-directed mutagenesis of the skeletal muscle channel, μ1 (Trimmer et al., 1989), was performed as previously described (Backx et al., 1992). A 1.9-kb *Bam*HI-*Sph*I cassette subcloned into pGEM-11 (Promega, Madison, WI) was used to introduce the point mutation at position *I*-53 (nomenclature of Tomaselli et al., 1993a; residue 402 in the amino acid sequence of the μ1 clone) with oligonucleotide-directed mutagenesis followed by phenotypic selection (Kunkel, 1985). The cassette was cloned into μ1 in pSP64T (Krieg and Melton, 1984) for in vitro transcription of cRNA and expression in *Xenopus* oocytes. All mutants were verified by DNA sequencing (Sanger et al., 1977; Sequenase, USB).

The whole-cell experiments were performed with oocytes injected with the α-subunit alone unless otherwise specified. Plasmids containing the wild-type or mutant μ1 Na channel α-subunits were linearized with *Sal*I, the β1 subunit (Isom et al., 1992) was linearized with *Eco*RI, and runoff RNA transcription was performed as previously described (Backx et al., 1992). Oocytes were injected with 50 nl of a 0.1–0.25 μg/μl RNA-containing solution. Oocytes co-injected with α and β1 cRNAs exhibited increased current density and were used in the single-channel experiments.

Oocytes were harvested from human chorionic gonadotrophin-primed adult female frogs (*Xenopus* I, Ann Arbor, MI, or Nasco, Ft. Atkinson, WI). Single oocytes were isolated by digestion of lobes of ovary in 1–2 mg/ml collagenase (Type IA, Sigma Chemical Co., St. Louis, MO) in calcium-free frog Ringer's solution. The oocytes were stored in frog Ringer's solution containing (in mM): 96 NaCl, 2 KCl, 1.8 $CaCl_2$, 1 $MgCl_2$, 5 *N*-(2-hydroxyethyl)piperazine-N′-(2-ethanesulfonic acid) (HEPES), pH 7.6, supplemented with penicillin (100 U/ml), streptomycin (100 μg/ml), 2 mM sodium pyruvate, and 0.5 mM theophylline. In preparation for patch clamp recording, the visceral vitelline membrane was manually removed after incubation of the oocyte in a hypertonic solution containing (in mM): 220 *N*-methyl-D-glucamine (NMG), 220 aspartic acid, 2 $MgCl_2$, 10 HEPES, 10 ethylene glycol-bis(β-amino-ethyl ether)-*N,N,N′,N′*-tetraacetic acid (EGTA), pH 7.2.

Electrophysiology

Whole-oocyte currents were recorded with a two-microelectrode voltage clamp (OC-725B, Warner Instrument Corp., Hamden, CT) 2–5 days after RNA injection. Intracellular microelectrode resistances were 0.5–1 MΩ when filled with 3 M KCl. Currents were measured in modified frog Ringer's solution containing (in mM): 96 NaCl, 2 KCl, 1 $MgCl_2$, 5 HEPES, pH 7.6. The monovalent cations Li^+, Cs^+, K^+, NMG^+, and NH_4^+ replaced Na^+ as chloride salts (Sigma) for the whole-cell selectivity measurements. To optimize voltage control, we used oocytes with small currents (<5 μA). Oocytes exhibiting an abrupt rise in the negative slope region of the current-voltage relationship or notches in the current records were not used for whole-cell experiments. Dose-response curves for tetrodotoxin (TTX) and Cd^{2+} (Sigma) were constructed from peak currents measured after bath application of the blocking agent alternating with washes by control solution. Steady-state inactivation was determined by using one second prepulses from −110 to −30 mV in decrements of 10 mV preceding a test pulse to −20 mV. To avoid cumulative inactivation, a repetition interval of 8 s for wild-type channels and 2 s for *I*-W53C channels was employed. We observed no voltage shift in the steady-state inactivation curves over the time course of these experiments (~10 min).

Whole-cell currents were sampled at 5 kHz through a 12 bit A/D converter (model TL-1 DMA Labmaster, Axon Instruments, Foster City, CA) and low-pass filtered at 1–2 kHz (−3dB) with an 8-pole Bessel filter (Frequency Devices, Haverhill, MA). The currents were acquired and analyzed with custom-written software.

Single-channel currents were measured with the cell-attached or inside-out excised configurations of the patch clamp (Hamill et al., 1981) with an Axopatch 200A amplifier (Axon Instruments, Burlingame, CA). The currents were sampled at 10 kHz and low-pass filtered at 1 kHz. The pipette solution contained (in mM): 140 NaCl, 10 HEPES, 1 $BaCl_2$, pH 7.4. The bath contained either the same Na^+ solution (inside-out patches) or (in mM): 140 KCl, 10 HEPES, pH 7.4 (cell-attached patches). The unitary currents were modified by bath application of 20 μM fenvalerate (DuPont, Wilmington, DE) for analysis of open-channel blockade by Cd^{2+} as previously described (Backx et al., 1992). All experiments were performed at 20–22°C.

Data analysis

Whole-cell current-voltage relationships were fit with a function combining the Boltzmann distribution describing steady-state activation and the Goldman-Hodgkin-Katz constant field equation (Hille, 1992).

Dose-response relationships were fit with a logistic function. Steady-state inactivation curves were generated by a two-pulse protocol, and the normalized peak currents were fit with a Boltzmann function. The best-fit curves to the data were determined by a nonlinear least-squares method (Levenberg-Marquardt algorithm, Origin, MicroCal, Northhampton, MA). The rate of whole-cell current decay was estimated by measuring the time from the peak to 50% decay of the current to permit model-independent comparisons among oocytes. The time courses of macroscopic current decay were compared only for oocytes with similar current densities (peak currents of 1–4 μA).

Single-channel opening events were determined by using a half-height criterion (Colquhoun and Sigworth, 1983). Amplitude histograms were fit-

ted to the sum of Gaussians by using a nonlinear least-squares method. One- to three-channel patches were used for generation of the open time histograms of unmodified channels; with multi-channel patches, openings were randomly assigned to closures. Open time histograms were fit with single-exponential functions. We made no correction for missed events and estimate for the shortest openings a missed event rate of 20% (Blatz and Magelby, 1986). However, failing to correct for missed events would result in an underestimation of the difference between the wild-type channels and the mutant.

Single-channel analysis of Cd^{2+} blockade was performed on channels modified with fenvalerate to remove the confounding effects of fast inactivation. The voltage dependence of Cd^{2+} blockade of the pore was determined by assuming a single-site binding model as previously described (Woodhull, 1973, Backx et al., 1992). The integral of the current through the open channel in the presence of Cd^{2+} was used to determine the average blocked unitary current amplitude. A linear transformation of the voltage dependence of the ratio of the blocked and unblocked current amplitudes is:

$$\ln\left(\frac{i_c}{i_b} - 1\right) = \ln K_A \times [Cd^{2+}] - \delta\frac{zFV}{RT}$$

where K_A is the association constant, i_c is the unblocked and i_b is the blocked single-channel current amplitude, and δ is the fractional electrical distance from the outer face of the membrane, and z, F, R, and T have their usual meanings. The slope of the log-linear plot gives the δ. The data were fit by least-squares linear regression (Origin, MicroCal).

Pooled data are expressed as the means and standard deviations, and statistical comparisons were made by one-way analysis of variance (ANOVA) unless otherwise specified.

Modeling and rate constant estimation

To understand how this mutation (*I*-W53C) altered gating transitions of the Na channel, ensemble average data were fit with a gating model similar to that recently implemented by Kuo and Bean (1994) with the addition of a second inactivation particle. Channel opening in this model results from activation of four identical and independent gating sensors, followed by an additional opening step. Inactivation can result from block of any closed (C_x) or open (O) state of the channel by either inactivation particle (I_1 or I_2), but the affinity of the channel for the inactivation particles increases progressively as more gating sensors are activated. Microscopic reversibility requires that the gating kinetics of the channel be altered when the inactivation particles are bound (hence the a and b factors). In the model, the OI_1 and OI_2 states are nonconducting; O is the only conducting state, and binding of the two inactivation particles is mutually exclusive.

$$\begin{array}{ccccccccccc} & 4\alpha b & & 3\alpha b & & 2\alpha b & & \alpha b & & \gamma & \\ C_1I_2 & \rightleftharpoons & C_2I_2 & \rightleftharpoons & C_3I_2 & \rightleftharpoons & C_4I_2 & \rightleftharpoons & C_5I_2 & \rightleftharpoons & OI_2 \\ & \beta/b & & 2\beta/b & & 3\beta/b & & 4\beta/b & & \delta & \end{array}$$

$$k_5\downarrow\uparrow k_6 \qquad k_5/b\downarrow\uparrow k_6 b \qquad k_5/b^2\downarrow\uparrow k_6 b^2 \qquad k_5/b^3\downarrow\uparrow k_6\, b^3 \qquad k_5/b^4\downarrow\uparrow k_6 b^4 \qquad k_7\downarrow\uparrow k_8$$

$$\begin{array}{ccccccccccc} & 4\alpha & & 3\alpha & & 2\alpha & & \alpha & & \gamma & \\ C_1 & \rightleftharpoons & C_2 & \rightleftharpoons & C_3 & \rightleftharpoons & C_4 & \rightleftharpoons & C_5 & \rightleftharpoons & O \\ & \beta & & 2\beta & & 3\beta & & 4\beta & & \delta & \end{array}$$

$$k_1\downarrow\uparrow k_2 \qquad k_1/a\downarrow\uparrow k_2 a \qquad k_1/a^2\downarrow\uparrow k_2 a^2 \qquad k_1/a^3\downarrow\uparrow k_2 a^3 \qquad k_1/a^4\downarrow\uparrow k_2 a^4 \qquad k_3\downarrow\uparrow k_4$$

$$\begin{array}{ccccccccccc} & 4\alpha a & & 3\alpha a & & 2\alpha a & & \alpha a & & \gamma & \\ C_1I_1 & \rightleftharpoons & C_2I_1 & \rightleftharpoons & C_3I_1 & \rightleftharpoons & C_4I_1 & \rightleftharpoons & C_5I_1 & \rightleftharpoons & OI_1 \\ & \beta/a & & 2\beta/a & & 3\beta/a & & 4\beta/a & & \delta & \end{array}$$

$$a = [(k_1/k_2)/(k_3/k_4)]^{1/8} \qquad b = [(k_5/k_6)/(k_7/k_8)]^{1/8}$$

Details of the parameterization of the rate constants and fitting procedure have been previously reported; the routine is similar to that used by Balser et al. (1990a,b) for fitting a gating model to ensemble average or whole-cell currents. Briefly, the fitting routine finds a set of rate constants that minimizes the difference between the calculated occupancy of the open state and the ensemble average current expressed as an open probability. We fit two gating models with identical structure but with specific rate constants differing on the basis of the presence of the mutation. To find a global minimum, an algorithm was developed that allowed fitting of both *I*-W53C and wild-type data simultaneously. All of the inactivation (vertical: k_1–k_8) rate constants were constrained to be identical for the wild-type and *I*-W53C data sets, whereas the activation/deactivation (horizontal: α, β, γ, δ) rate constants were allowed to differ. Mean open times determined from single-channel experiments were used to constrain the rate constants for exiting the open state (δ, k_4, k_8).

The fitting program was implemented in NDP FORTRAN (Microway, Keystone, MA). A numerical integrator was used to calculate the open-state occupancy for a given set of rate constants (LSODA; Hindmarsh, 1983; Petzold, 1983). The calculated open-state occupancy was compared with the experimental data, and the parameters were updated with a SIMPLEX algorithm (Nelder and Mead, 1965) to minimize the sum of squared errors.

RESULTS

Cysteine substitution in the first domain alters the permeation phenotype

Selectivity

The presence of a cysteine at relative position 52 in the S5-S6 linker (Tomaselli et al., 1993a) of the first domain of the Na channel is associated with sensitivity to block by group IIB divalent cations and resistance to TTX (Satin et al., 1992a; Backx et al., 1992; Fig. 1). In an effort to define which residues of the S5-S6 linker (P-loop) participate in formation of the pore of the channel, we replaced other amino acids in this region with cysteine. We reasoned that the mutant, cysteine-substituted channels would exhibit increased Cd^{2+} sensitivity, if and only if the thiol side chain points into the pore. Substituting different residues in the linear amino acid sequence would then move the Cd^{2+} binding site within the electrical field, permitting the correlation of physical distances with electrical distances.

Substitution of the highly conserved tryptophan at position 53 of the domain *I* S5-S6 linker with cysteine produced a functional, Na^+-selective channel with altered sensitivity to Cd^{2+} and TTX compared with the wild-type channel. Whole-cell currents elicited by depolarizing voltage steps in an oocyte injected with the wild-type or mutant α-subunit *I*-W53C are shown in Fig. 2 *A*. The *I*-W53C current activates during depolarizing steps positive to −50 mV and peaks at −25 mV, approximately 5 mV more negative than wild-type currents measured under identical conditions (Fig. 2, *B* and *C*). Determination of the reversal potential was not reliable for two reasons. First, voltage steps to positive potentials hasten the time to peak, making the current measurements inaccurate. Second, the positive slope region of the whole-cell current-voltage relationship was nonlinear, particularly for the mutant channel (Fig. 2, *B* and *C*).

The expressed wild-type and *I*-W53C channels are Na^+ selective, although the two channels differ in their relative Li^+ permeabilities. Plots of the peak inward current in bath solutions with different monovalent cations are shown for the wild-type and mutant channel in Fig. 3 *A*. The peak currents in 96 mM K^+, Cs^+, NH_4^+, and NMG^+ are <5% of the currents in Na^+. The wild-type peak current in 96 mM Li^+ is 65 ± 4% (n = 3) of that in 96 mM Na^+, whereas the peak current

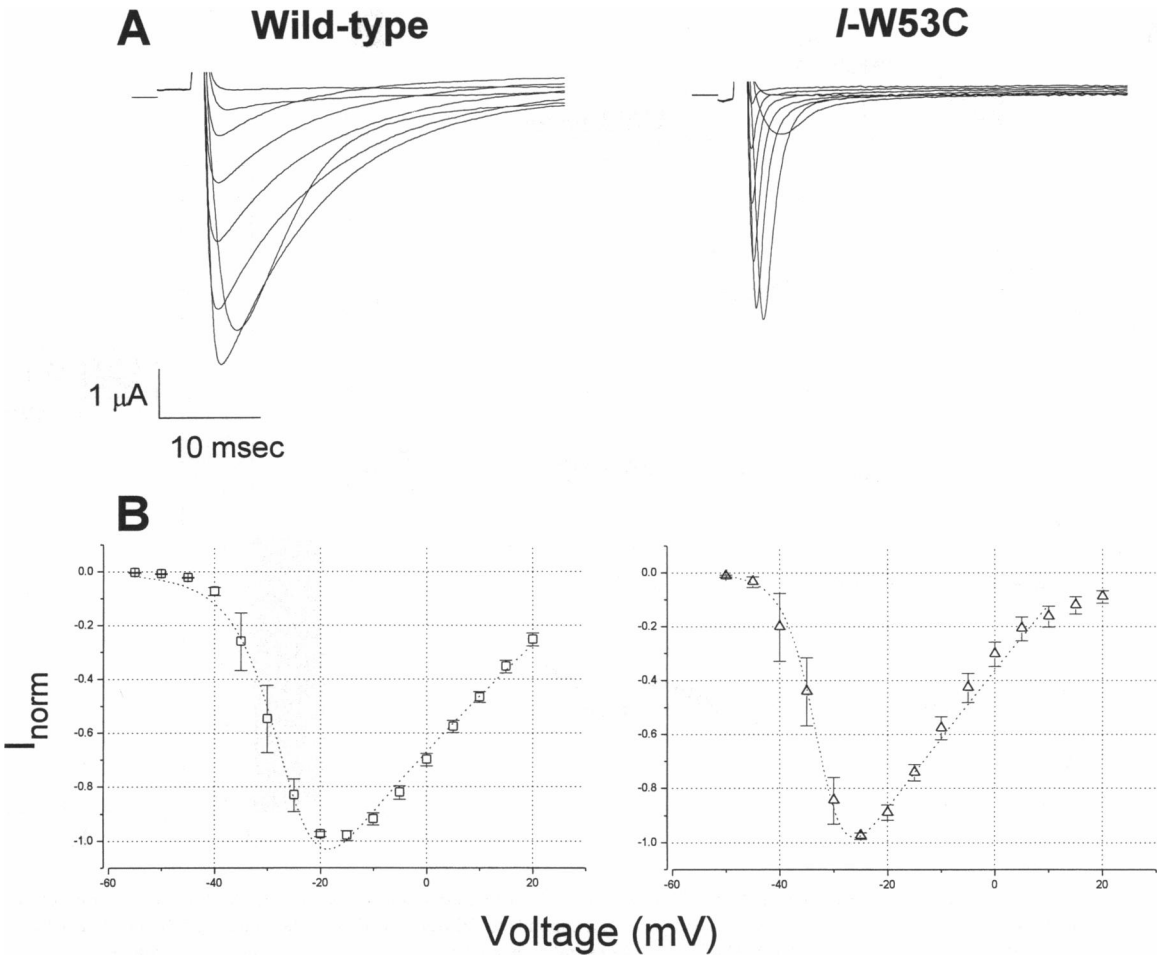

FIGURE 2 *I*-W53C mutation produces functional Na^+-selective channels. (*A*) Representative non-leak-subtracted whole-cell currents recorded from a *Xenopus* oocyte injected with wild-type μ1 (left) and mutant *I*-W53C (right) cRNA. The horizontal lines to the left of each set of currents represents the zero current level. (*B*) Current-voltage relationships normalized to the peak current. The dotted lines are fits to the data between −55 and +20 mV with a function combining the Goldman-Hodgkin-Katz constant field equation and a Boltzmann distribution describing the steady-state activation. On the left is the wild-type (n = 4) and on the right is *I*-W53C (n = 6). The mutant channel activates and peaks 7–10 mV more hyperpolarized than the wild-type channel.

of the *I*-W53C mutant in Li^+-containing bath solution is 153 ± 29% (n = 3) of that in Na^+. The peak current data for Li^+ and K^+ are summarized in the form of a bar plot in Fig. 3 *B*; the peak Li^+ currents are significantly larger in the mutant compared with the wild-type channel ($p < 0.001$). This change in selectivity is the first piece of evidence that the substituted cysteine is within the pore. We next examined blockade by divalent cations and toxin.

Blockade by Cd^{2+} and tetrodotoxin

The site of the cysteine substitution *I*-W53C is adjacent to a naturally variant residue at position 52, which is a cysteine in the cardiac isoform of the channel and a tyrosine or phenylalanine in the skeletal muscle and brain isoforms, respectively (Noda et al., 1986; Auld et al., 1988; Trimmer et al., 1989; Rogart et al., 1989). A cysteine at position *I*-52 is associated with sensitivity of the channel to blockade by Cd^{2+}, and resistance to blockade by guanidinium toxins such as TTX. We evaluated the sensitivity of *I*-W53C to Cd^{2+} and TTX to determine whether this cysteine substitution mutant also renders the channel sensitive to blockade by Cd^{2+} and resistant to TTX. Compared with the Cd^{2+}-resistant wild-type channel and the Cd^{2+}-sensitive mutant *I*-Y52C, *I*-W53C exhibits intermediate susceptibility to blockade by Cd^{2+}. The IC_{50} for blockade of this mutant by Cd^{2+} is 114 ± 18 μM compared with 17 ± 2 μM and 3.3 ± 1.7 mM at a test potential of −20 mV for the *I*-Y52C mutant and the wild-type channel, respectively (Fig. 4 *A*). The sensitivity of native skeletal muscle and cardiac Na channels to TTX is reciprocally related to their Cd^{2+} affinity (Frelin et al., 1986); analogously, the *I*-Y52C mutant, which is quite sensitive to blockade by Cd^{2+}, is very resistant to TTX (Backx et al., 1992; Satin et al., 1992a). The dose-response curves to TTX (Fig. 4 *B*) illustrate that *I*-W53C again has an intermediate sensitivity and is half-blocked by 595 ± 150 nM TTX; the wild-type channel has an IC_{50} of 15 ± 0.7 nM, whereas the *I*-Y52C mutant is extremely resistant, being blocked only

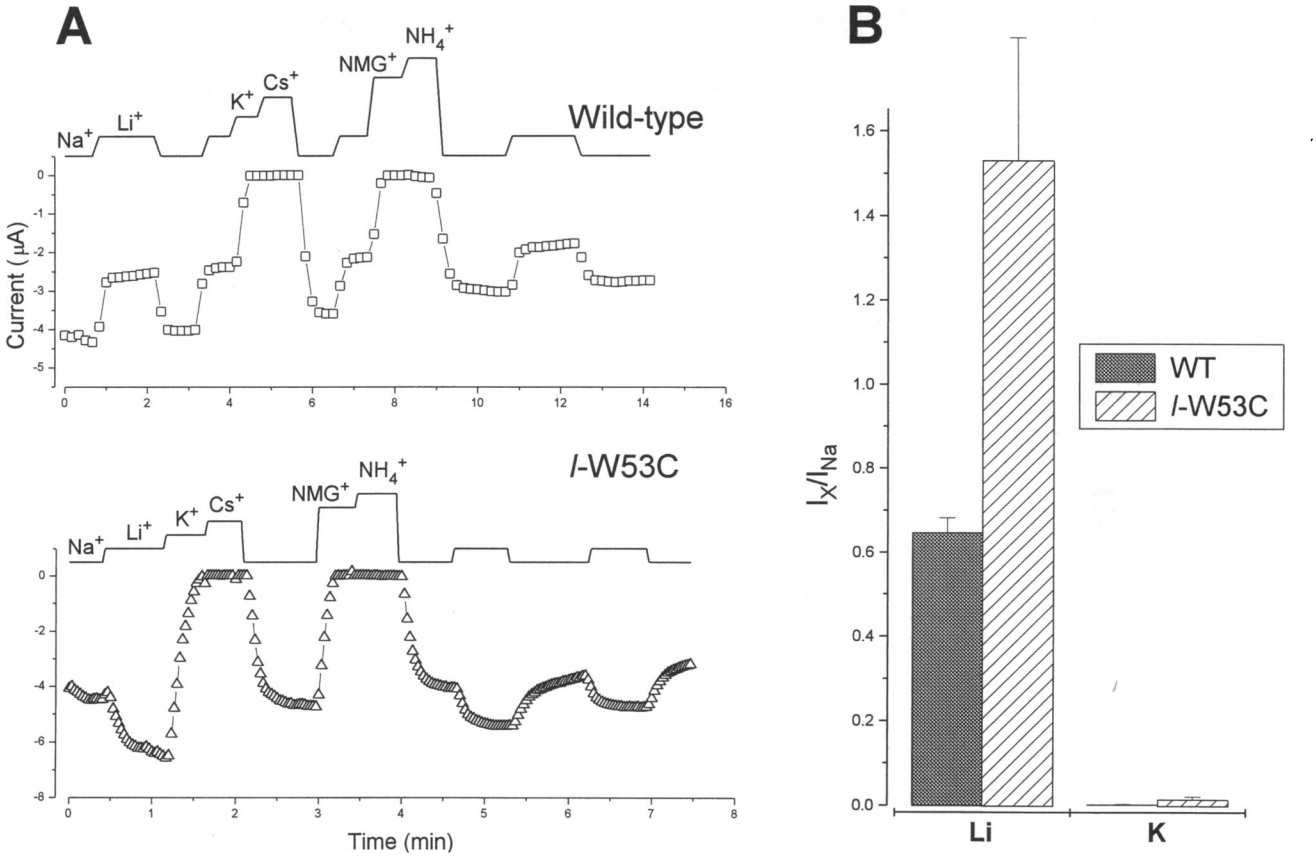

FIGURE 3 Monovalent cation selectivity of the channels. (*A*) Plots of the peak current amplitudes in changing 96 mM cationic solution. In each plot the lines above the symbols represent the solution changes, and each level corresponds to a different cation-containing bath solution. The wild-type channel (top) is depolarized from −100 to −20 mV every 8 s. *I*-W53C is subjected to similar changes in bath solution, and depolarizing voltage steps are made every 2 s. The wild-type channel has a larger peak current in Na^+ than Li^+; the reverse is true for the mutant. Neither variant is significantly permeable to K^+, Cs^+, NMG^+, or NH_4^+. (*B*) Bar graph of the peak currents relative to the peak current in Na^+ for the wild-type (shaded; $n = 3$) and *I*-W53C (hatched; $n = 3$)

40% by 50 μM TTX. The effects of *I*-W53C on Na^+ and Li^+ permeability, and the potencies of blockade of the channel by Cd^{2+} and TTX are all consistent with a location of this residue in the pore of the channel.

To determine the depth of the substituted cysteine in the pore, we examined the voltage dependence of blockade of the unitary current of *I*-W53C by Cd^{2+}. To facilitate these experiments, channel openings were prolonged by fenvalerate (Holloway et al., 1989, Backx et al., 1992). Fig. 5 *A* shows unitary currents recorded in the excised inside-out patch configuration. In the absence of divalent cations with symmetrical concentrations of Na^+ on both sides of the membrane, the channel openings are long and uninterrupted by closures. In the presence of 200 μM Cd^{2+}, *I*-W53C channel openings are interrupted by incompletely resolved blocking events (Fig. 5 *A*). The average unitary current amplitude plotted against voltage highlights the voltage dependence of the blockade (Fig. 5 *B*). The slope of the plot of the logarithm of the ratio of the blocked and unblocked currents predicts a fractional electrical distance (δ) of approximately 0.18 from the external side of the membrane (Fig. 5 *C*). This value is smaller than that estimated for Cd^{2+} blockade of the *I*-Y52C mutation ($\delta = 0.24$), consistent with the idea that residue *I*-53 lies external to *I*-52 in the P-loop (Backx et al., 1992; Tomaselli et al., 1993a). The mutant channel *I*-W53C alters the affinity of the channel for Cd^{2+} and is blocked by this divalent cation in a voltage-dependent fashion from the extracellular surface of the membrane. The alterations in Li^+ permeability, single-channel conductance, and Cd^{2+} blockade all imply that this residue lies within the pore; thus, the finding that this cysteine substitution altered channel gating was unexpected.

I-W53C channel alters gating

Kinetics of macroscopic currents

Na channel α-subunits expressed in *Xenopus* oocytes produce a whole-cell current that decays slowly compared with Na current in native tissue. Current decay is hastened in the presence of the β1 subunit (Isom et al., 1992; Cannon et al., 1993) and when the α-subunit is expressed in mammalian cells (Scheuer et al., 1990., Zhou et al., 1991). In addition to modifying pore properties, the mutation *I*-W53C alters macroscopic gating of the channel. Fig. 6 *A* shows superimposed, normalized currents recorded from oocytes injected with

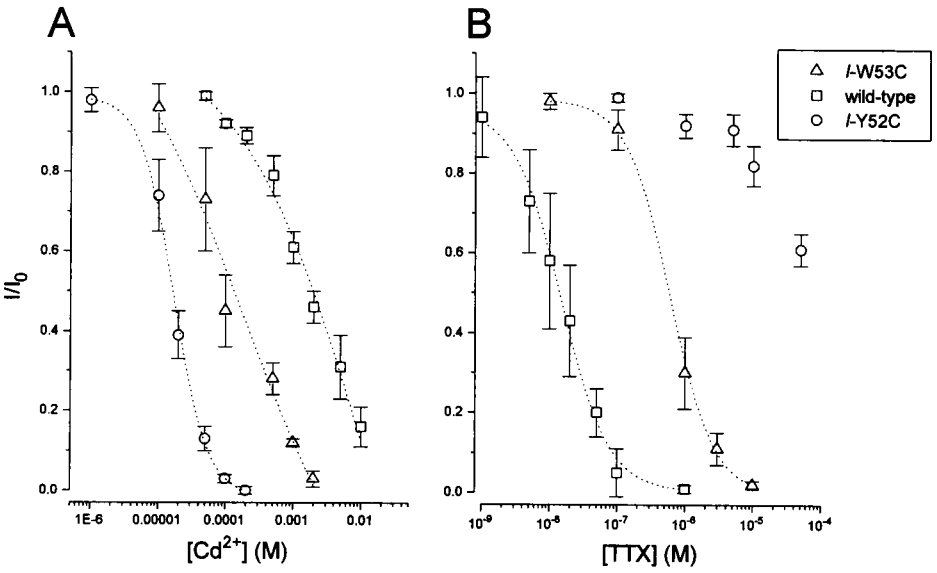

FIGURE 4 Whole-cell dose-response curves to Cd^{2+} and TTX. (*A*) The peak currents normalized to the current in the absence of Cd^{2+} for each Na channel variant is plotted; the dotted lines are weighted fits to a function of the form: $I/I_0 = 1 - (\max - \min)/(IC_{50} + [X])$, where X is either Cd^{2+} or TTX. The data for wild-type (squares; IC_{50} = 3.3 ± 1.7 mM; n = 6), *I*-W53C (triangles; IC_{50} = 114 ± 18 μM; n = 4), and *I*-Y52C (circles; IC_{50} = 17 ± 2 μM; n = 8) are shown. (*B*) Similar data and fits for TTX blockade of the wild-type (squares; IC_{50} = 15.0 ± 0.7 nM; n = 8), *I*-W53C (triangles; IC_{50} = 595 ± 150 nM; n = 7), and *I*-Y52C (circles; n = 4).

wild-type or *I*-W53C mutant α-subunit cRNA. Two effects are evident: first, the time to the peak of the current is shortened; second, the rate of decay of the whole-cell current is hastened. The times from the peak to 50% decay of the current ($t_{50\%}$-t_{peak}) are plotted in the bar graph (Fig. 6 *B*). The data compiled in this bar graph come from more than 10 rounds of injection for the wild-type and *I*-W53C mutant. Comparisons of the time course of whole-cell current decay were made in oocytes with similar current densities and generally in oocytes from the same frogs. The wild-type channel $t_{50\%}$-t_{peak} is 5.6 ± 1.9 and does not differ from that of other cysteine substitutions (*I*-Q50C, *I*-Y52C) in the first domain. In contrast, the *I*-W53C mutant has a $t_{50\%}$-t_{peak} of 1.5 ± 0.9 ms, significantly shorter than the other channel variants (p < 0.0001).

The changes in gating in Fig. 6, *A* and *B*, are not subtle. Nevertheless, whole-cell Na currents in oocytes are difficult to clamp given the rapid kinetics and the large membrane surface area that must be charged during the voltage step. Additional ambiguity is introduced by the variability of Na current decay, which is known to occur when only the α-subunit is injected into oocytes (Zhou et al., 1991). For these reasons, we confirmed that the differences in gating persist when Na currents are recorded from patches in oocytes co-injected with α and β1 subunits. Fig. 6 *C* shows ensemble average currents recorded from patches with three to four channels in each patch. As in the whole-cell recordings, the time to peak is shorter and the current decay is faster in the mutant compared with the wild-type channel.

The steady-state availability of the Na channel is shifted by the *I*-W53C mutation. The voltage dependence of steady-state inactivation was determined by plotting the normalized peak current against the prepulse potential. To achieve steady state, the durations of the prepulse potentials were 8 and 2 s for the wild-type and *I*-W53C channels, respectively. The midpoint and slope factors of the steady-state availability curves were 65 ± 6 mV and −74 ± 3 mV and 6 ± 1 mV and 4 ± 1 mV for the wild-type (n = 10) and *I*-W53C (n = 8) channels, respectively (Fig. 6 *D*, Table 1).

Single-channel recordings

The whole-cell data indicate that the mutation *I*-W53C affects both macroscopic activation and inactivation. To examine in detail the effects of this mutation on gating kinetics, we used single-channel recording. Fig. 7 *A* shows representative sweeps of channel openings during steps from a holding potential of −120 mV to a test potential of −30 mV. Several effects of the *I*-W53C mutation on the single-channel current are evident. First, the mutant channel has a smaller slope conductance than the wild-type (25 ± 0.5 versus 34 ± 1 pS, cell-attached; Fig. 7 *B*). Second, the latency to first opening is shorter for the *I*-W53C mutant than the wild-type channel. Finally, the mutant channel opens briefly and most often only once per depolarizing epoch over a wide range of test potentials, whereas wild-type channels typically reopen before inactivating.

The whole-cell data demonstrated an abbreviation of the time to peak and an acceleration of current decay without a shift in the voltage dependence of gating of the *I*-W53C mutation. We sought to examine the single-channel correlates of these findings. We analyzed the first latencies and mean open times of the wild-type and *I*-W53C channels over a range of test potentials. The mean open times, determined by single exponential fits to cumulative open time histograms,

TABLE 1 Steady-state inactivation gating parameters

	$V_{0.5}$	Slope factor	n
Wild-type, no β1	−65 ± 6	6.4 ± 1	10
Wild-type + β1	−67 ± 2	4.4 ± 1	4
I-W53C, no β1	−74 ± 3*	4.1 ± 0.3	8
I-W53C + β1	−72 ± 4‡	4.8 ± 1	9

*p = 0.006, ‡p = 0.03 versus wild-type.

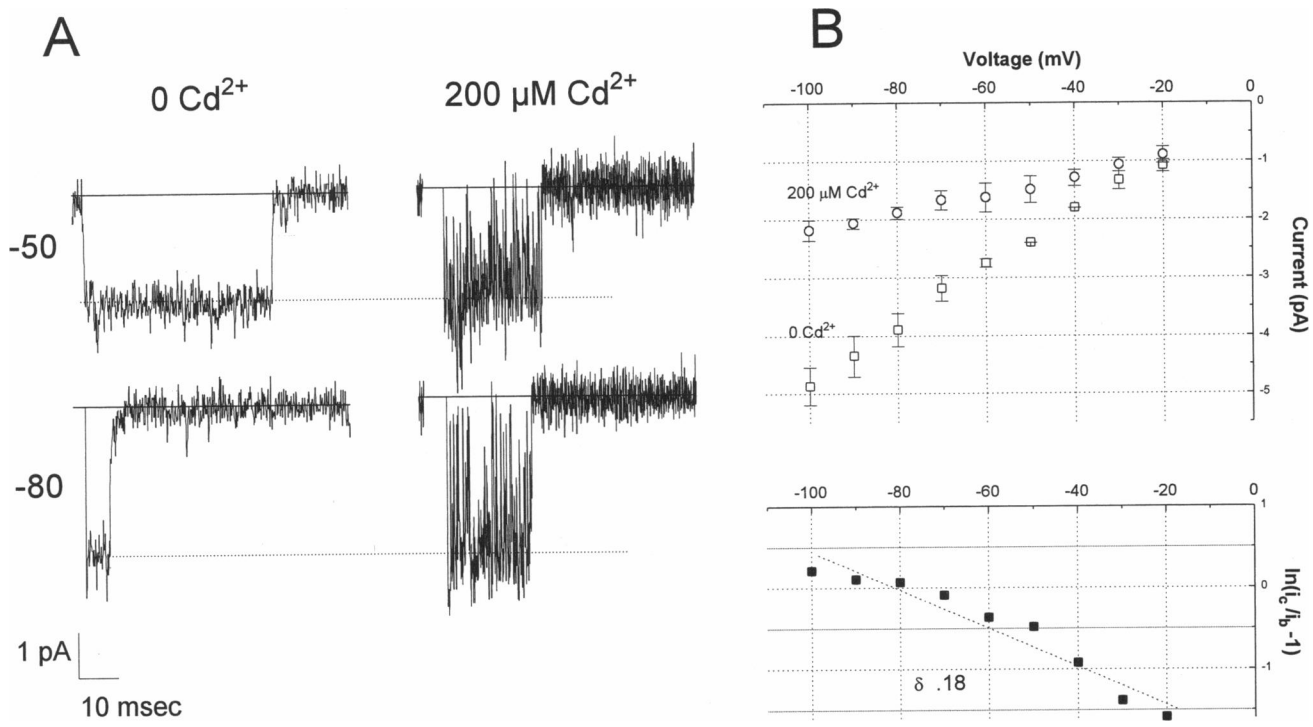

FIGURE 5 Cd^{2+} block of single *I*-W53C channels. (*A*) Representative single-channel current records to the designated potentials are shown. The currents have had fast inactivation removed by bath application of 20 μM fenvalerate. On the left are the currents in the absence of divalent cations. The currents on the right exhibit incompletely resolved blockade by 200 μM Cd^{2+}. (*B*, top) Single-channel current amplitude of the mutant *I*-W53C plotted against voltage in the absence (squares; $n = 3$) and the average unitary current in the presence (circles; $n = 3$) of Cd^{2+}, demonstrating the voltage dependence of the blockade. In the absence of divalent cations and excised patches with symmetrical Na^+ across the membrane, the slope conductance of the mutant is 46 ± 1 pS compared with 52 pS for the wild-type channel (Backx et al., 1992). (*B*, bottom) Plot of the logarithm of the blocked and unblocked unitary current amplitudes against voltage. As described in Materials and Methods, the slope of the line predicts a fractional electrical distance (δ) of 0.18.

demonstrate short open times of the mutant channel at hyperpolarized test potentials. Although the open time of the wild-type channel becomes longer at more depolarized potentials, *I*-W53C open time is invariant with voltage (Fig. 7 *C*). A decrease in the mean open time with voltage might not be detected because of the increased frequency of missed events, but certainly no increase in mean open time with voltage is observed in this mutant. Fig. 7 *D* shows representative cumulative first latency histograms of the mutant at four test potentials. The first latencies are uniformly short with the following times to 90% of the plateau: 1.02 ms (−60 mV), 0.73 ms (−50 mV), 1.25 ms (−40 mV), and 0.5 ms (−30 mV). Compared with the wild-type channel, the mutant channel exhibits a short first latency with reduced voltage dependence. The mutant channel also displays a greater percentage of blank sweeps (Fig. 7 *E*).

In summary, the *I*-W53C channels open with a short latency and do so briefly and typically only once per depolarizing epoch. This contrasts with microscopic gating of the wild-type channels, in which open times increase with depolarizing voltage steps and reopening is frequent, especially at negative test voltages. The very short first latencies imply a change in the microscopic activation rates, but can all of the changes in the currents be explained by altered activation or are changes in microscopic inactivation also required? For example, the brief, voltage-independent mean open times could reflect a dominance of the inactivation rate at all voltages or a shift in the voltage dependence of the inactivation rate to more hyperpolarized potentials (Yue et al., 1989). Alternatively, hastening activation rates in the setting of inactivation that is not rate-limiting might be capable of accounting for all of the changes in the current kinetics (Aldrich et al., 1983).

Gating model of *I*-W53C

To interpret the changes produced by this mutation, we have implemented a contemporary gating model (Kuo and Bean, 1994) to fit ensemble average currents of wild-type and *I*-W53C Na channel α-subunits coexpressed with β1. The peak P_{open} and mean open times were used to scale the ensemble average currents into P_{open} and constrain the fitting procedure as described in the Methods. We used a peak P_{open} for wild-type (α plus β1) single channels of 0.21 and a mean open time of 0.3 ms at −40 mV (P. Backx, unpublished observation); for *I*-W53C, a peak P_{open} of 0.27 and a mean open time of 0.19 ms were used. Two competing inactivation particles (or processes) were employed to account for the distinct rapid and slow whole-cell decay kinetics and biexponential recovery from inactivation observed for skeletal muscle Na channels. Inactivation rate constants were constrained to remain identical for fitting both wild-type and

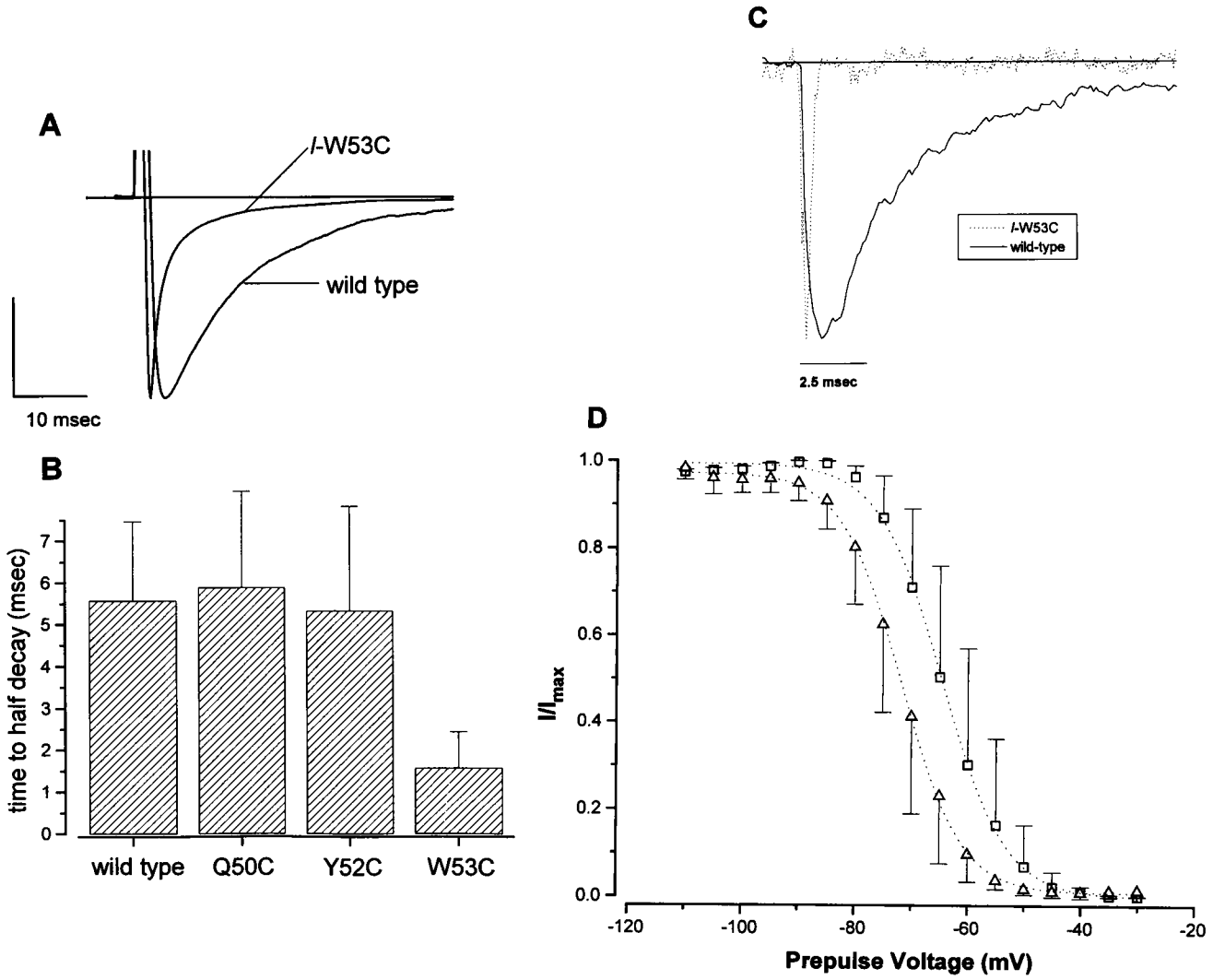

FIGURE 6 Gating of *I*-W53C is altered. (*A*) Plots of whole-cell currents normalized to their peaks. The voltage protocol is a step from −100 to −20 mV. The mutant peaks faster and decays faster than the wild-type channel. (*B*) Bar graph of the time from the peak to 50% current decay for the wild-type channel and a number of cysteine substitution mutants in the first domain. The time from peak to 50% current decay were: wild-type, 5.6 ± 1.9 (n = 29); *I*-Q50C, 5.9 ± 2.3 (n = 5); *I*-Y52C, 5.3 ± 2.5 (n = 11); *I*-W53C, 1.6 ± 0.87 (n = 35). Records with similar peak currents were analyzed. The peak currents were 4.5 ± 3 and 3.8 ± 3.4 μA for the wild-type and mutant channels, respectively. (*C*) Ensemble average currents with β1 coexpression, generated from single patches of each variant containing 3–4 channels. The patches were held at −120 mV and stepped to −40 mV. The ensemble averages reconstitute the acceleration of the time to peak and hastening of the mutant current decay observed in whole-cell recordings. (*D*) Steady-state inactivation curves for the wild-type (squares) and mutant (triangles) channels. The steady-state availability of *I*-W53C is shifted 7 mV in the hyperpolarizing direction. Wild-type, −64.9 ± 6 mV (n = 10); *I*-W53C, −74 ± 2.7 (n = 8); p = 0.006.

I-W53C data, but the activation and deactivation rate constants (O, β, γ, δ) were allowed to differ. Fig. 8 *A* shows the least-squares fit (solid lines) to ensemble average currents recorded at −40 mV from a wild-type patch having three channels (circles) and an *I*-W53C patch having five channels (squares). Accurate leak subtraction during the first 350 ms of the voltage step was difficult, so data from this time were not included in the fit. During the late decay phase of the wild-type ensemble average, fewer data points were selected for fitting to equalize the *I*-W53C and wild-type data sets for weighting purposes. The resulting fitted rate constants are summarized in Table 2.

The peak Na current occurs much earlier for *I*-W53C than for the wild-type channel (Fig. 8 *A*), the result of a shortened latency to first opening for the mutant. The fitted rate constants are consistent with this behavior. Because the final gating transition in channel opening is rapid ($\gamma > 10^5$), activation of the four gating sensors is rate limiting ($\alpha \sim 10^3$). The *I*-W53C forward rate constant (α) is more than 3 times the wild-type rate constant, providing a forward rate more than 12 times greater than wild-type for the initial gating transition (see model). Notably, both the percentage of sweeps with openings and the frequency of openings during a step to −40 mV is markedly reduced for the *I*-W53C mutant and is reflected in the large reduction in the area under the ensemble average P_{open} curve (Fig. 8 *A*). This is largely a result of enhanced closed state inactivation. The rate constants favoring inactivation before opening (k_2 for the I_1 gat-

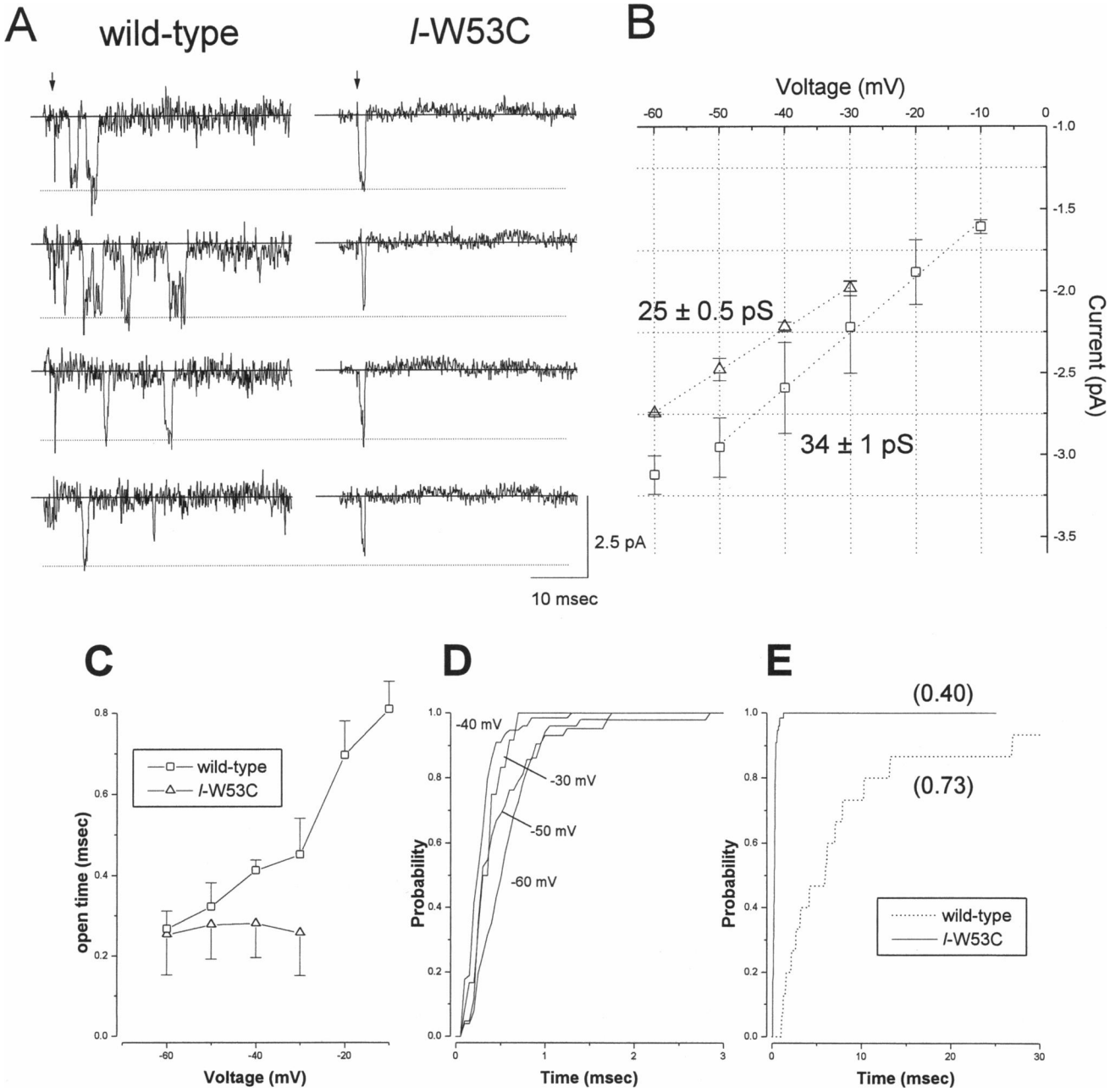

FIGURE 7 Single-channel properties of *I*-W53C. (*A*) Representative single-channel current records from cell-attached membrane patches of oocytes expressing the wild-type channel or *I*-W53C with coexpression of the β1 subunit. The membrane patches are held at −120 mV and pulsed to −30 mV. The arrows indicate the time of the depolarizing voltage step. The wild-type channels open with a variable first latency and often reopen during the depolarizing epoch. The mutant opens with a short first latency and opens only once during a 40-ms depolarizing pulse. (*B*) The single-channel current-voltage relationship demonstrates the smaller conductance of the mutant under these conditions. The slope conductance of the mutant may be underestimated because of the short mean open time. The data are from four *I*-W53C mutant and six wild-type patches. (*C*) Plot of the mean open time from single-exponential fits of the open time histogram from membrane patches. The data are from three patches of the wild-type and mutant channel. The mean open time of the wild-type channel increases with more depolarized test potentials up to −20 mV. *I*-W53C exhibits no significant change in open time with test potential. (*D*) Representative normalized cumulative first latency histograms from a patch containing three *I*-W53C channels. The latency to first opening is uniformly short over the voltage range −60 to −30 mV. At test potentials more positive than −30 mV, openings are buried in the capacity transient. (*E*) Representative cumulative first latency histogram for the wild-type and *I*-W53C channel, each from membrane patches containing three channels. These are the latencies to first opening for a depolarizing pulse to −30 mV. The numbers in parentheses are the percentages of sweeps with openings

ing particle, k_6 for the I_2 gating particle) compete with the forward rate constants (α, γ) to limit P_{open}. Although inactivation via binding of the I_2 gating particle to closed states is rare ($k_6 b^4 \rightarrow 0\ s^{-1}$), closed state affinity for the I_1 particle is high. The maximal rate for closed state inactivation is that of $C_5 \rightarrow C_5I_1$ ($k_2 a^4 = 4.0e^5\ s^{-1}$). Closed state inactivation via this pathway would explain the low P_{open} for both the wild-type and *I*-W53C channels; however, the fivefold reduction

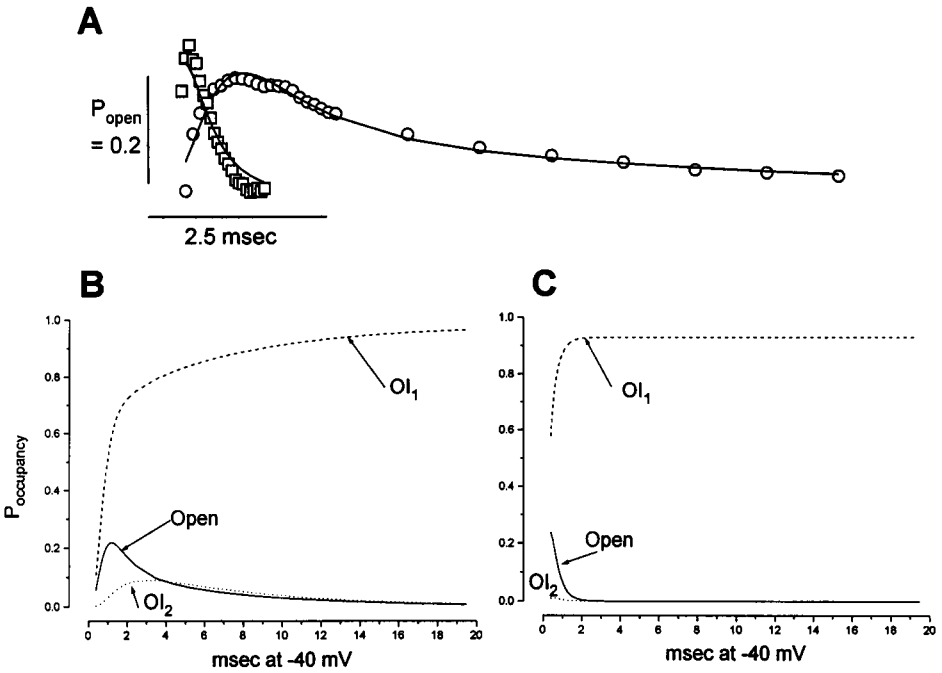

FIGURE 8 Gating model of the effect of the cysteine mutant *I*-W53C. (*A*) The solid lines are fits to wild-type (circles) and *I*-W53C (squares) ensemble average currents expressed as open probabilities. The fits are generated by constraining the inactivation rate constants and permitting activation rate constants to vary only between the wild-type and mutant channels. (*B*) In the wild-type channel, the slow decay in the average current tracks the occupancy of the nonabsorbing inactivated state (OI_2). (*C*) In the case of *I*-W53C, macroscopic current decay is brisk and the occupancy of the absorbing state (OI_1) is rapid.

in the $C_5 \rightarrow O$ activation rate for *I*-W53C (γ reduced from $3.7e^6$ s^{-1} to $7.3e^5$ s^{-1}) would markedly increase the probability of early inactivation from the C_5 state. The model prediction for the time course of entry into the two inactivated states for both wild-type (Fig. 8 *B*) and *I*-W53C channels (Fig. 8 *C*) highlight the coupling of activation and inactivation. Accumulation of channels in the OI_1 state is much more rapid for *I*-W53C channels because deactivation is accelerated, thereby creating more opportunities for the channel to inactivate from C_5.

The decay of the ensemble average current was faster for *I*-W53C than for the wild-type channel. This effect could be simulated without imposing any change in the inactivation (k_1–k_8) rate constants. This suggests that the hastening of whole-cell inactivation of the *I*-W53C mutation may result primarily from a change in microscopic activation. This may be understood as follows. The affinity of open channels for the OI_1 inactivation particle is very high ($k_4 \gg k_3$) and is therefore absorbing. In contrast, the O and OI_2 states are in rapid equilibrium (k_7 and k_8 are large and have similar magnitude), so that reopening from OI_2 may occur. Such reopening would slow the decay of ensemble average current, as shown in the Fig. 8 *B*. Note that occupancy of OI_2 tracks the occupancy of the O state during the decay phase, reflecting the rapid equilibrium between these states. Channels may flicker between the O and OI_2 states, causing late openings and prolonging the decay phase before permanently inactivating via entry into OI_1. In contrast, for *I*-W53C, shortening of the decay phase may be explained by two factors: first, the reduced likelihood of late openings is a result of a combination of a shortened first latency and increased closed channel inactivation (into OI_1); second, the mutant mean open time is reduced from 0.3 ms to 0.19 ms. If the mutation does not affect inactivation directly, δ ($O \rightarrow C_5$) must be increased for *I*-W53C to account for the reduction in mean open time. In the model, the open-time constraint resulted in a twofold increase in δ. Hence, mutant channels that reached the open state were more likely to reclose and inactivate via $C_5 \rightarrow I_1$ than enter the OI_2 nonabsorbing state. This would eliminate reopenings from OI_2 and explain the higher frequency of single openings seen in the *I*-W53C single-channel data (Fig. 7 *A*). Fig. 8 *C* shows the markedly reduced occupancy of the OI_2 state predicted by the model for *I*-W53C and the resultant elimination of slow decay. Therefore, the changes in gating produced by this mutation can be explained by a speeding of microscopic activation and deactivation rates without having to invoke any changes in microscopic inactivation rates.

TABLE 2 Gating model rate constants

	α	β	γ	δ
Wild-type (s^{-1})	1947	~0	$3.7\ e^6$	2815
I-W53C	6780	~0	$7.3\ e^5$	6255

a = 145; b = $6.5e^{-29}$
k_1, k_3, k_5 ~0
k_2 = $0.94e^{-3}$; k_4 = 50.1; k_6 = 145; k_7 = 437; k_8 = 361 s^{-1}.

DISCUSSION

Cysteine-scanning mutagenesis in the pore of the Na channel

The approach of using site-directed mutagenesis and membrane current recording has been exploited to study structure-function relationships in a wide array of ion channels. A limitation of this strategy is that changes in function produced by mutations may be difficult to interpret even with conservative amino acid substitutions. Nevertheless, the use of a cysteine substitution mutagenesis strategy in the study of ion channels has several at-

tractive features. First, substituted cysteines may form group IIB metal binding sites, if the sulfhydryl side chain is accessible to the pore. These metals are potent blockers of cardiac Na channels (Schild and Moczydlowski, 1991; Frelin et al., 1986). The thiol side chain of cysteine is a target for specific chemical modifying agents. Furthermore, single cysteine substitutions can suffice to confer high affinity metal binding (Satin et al., 1992a; Backx et al., 1992; Yellen et al., 1994) and sensitivity to sulfhydryl modifying agents (Akabas et al., 1992; Kurz et al., 1994) in ion channel proteins. We have previously described a single cysteine substitution in the pore of the mammalian skeletal muscle Na channel (*I*-Y52C) that alters Na^+ conductance and sensitivity to blockade by Cd^{2+} and TTX. The presence of a cysteine, the naturally occuring residue at this position in the cardiac isoform, is associated with a smaller single-channel conductance, enhanced sensitivity to blockade by Cd^{2+}, and resistance to TTX (Backx et al., 1992). We measured the voltage dependence of blockade of the single-channel currents to locate the Cd^{2+}-binding site, in which cysteine confers the high binding affinity, within the membrane electrical field. This observation led us to hypothesize that serial cysteine substitutions would suffice to increase the sensitivity to Cd^{2+} blockade if the thiol side chains of the substituted residues protrude into the pore. If such reasoning is correct, this strategy may enable us to map the extent and topology of the Na channel pore. Substitution of the adjacent tryptophan with cysteine in the first domain (*I*-W53C) produces a channel with intermediate sensitivity to blockade by both Cd^{2+} and TTX compared with the wild-type skeletal muscle and *I*-Y52C variants (Fig. 4). Moving the location of the cysteine within the pore alters the metal binding site, so it is not surprising that the Cd^{2+} affinity differs from both the wild-type channel and the *I*-Y52C mutation. This mutation also reduces the single-channel conductance compared with the parental, skeletal muscle channel (Fig. 7, *A* and *B*). *I*-W53C thus has a pore phenotype that is intermediate to that of the cardiac and skeletal muscle isoforms, which differ in the P-loop of the first domain by the presence of a cysteine versus an aromatic residue at position 52. By using blockade by Cd^{2+} and TTX as phenotypic features, serial replacement of residues in the P-loops of the Na channel may provide useful structural and topological information. A unique advantage of group IIB divalent cations is the possibility for locating substituted cysteines relative to the membrane electrical field (and each other) by analyzing the voltage dependence of blockade (Fig. 5). It is possible that other residues contribute to coordination of Cd^{2+} in the channel; e.g., other cysteines or histidines may be involved in metal binding (Lipkind and Fozzard, 1994; Doyle et al., 1993). Nevertheless, the affinity of cysteine pore mutants is relatively low for group IIB metals ($K_d \sim 10^{-5}$–10^{-4} M) compared with other proteins (e.g., zinc finger transcription factors, $K_d \leq 10^{-9}$ M) that contain multiple coordinated cysteines or histidines (Berg, 1990). Second, the ability to produce high affinity Cd^{2+} binding sites with individual widely dispersed cysteine substitutions in the P-loops of all four domains of the channel (Tomaselli et al., 1994) also favors an unconstrained binding site composed of a single thiol group.

General structural implications for the P-loop of the Na channel

We have shown that replacement of the amino acid at position *I*-53 in the S5-S6 linker alters various features of ion permeation and channel blockade. Amino acids at positions 51, 52, and 54 also affect permeation (Noda et al., 1989; Terlau et al. 1991; Pusch et al., 1991; Satin et al., 1992a; Backx et al., 1992). The presence of four consecutive residues with side chains that influence ion permeation and/or pore blockade of the Na channel is inconsistent with the anti-parallel β-sheet folding pattern proposed in earlier models of the pore (Guy and Seetharamulu, 1986; Backx et al., 1992; Lipkind and Fozzard, 1994). An α-helical conformation in this region is also excluded by the experimental data. Possible higher order structures for this region of the pore include a random coil or an antiparallel β-sheet with a plane that forms a wall of the pore, permitting the side chains of sequential residues to influence ions in the pore. The latter possibility seems less likely as the pore in such a structure would be lined more by the peptide backbone than by the side chains that make each residue unique. Nevertheless, we cannot rule out the possibility that substitution of the native residue with cysteine produces a local disruption of the protein structure such that the thiol side chain remains exposed to the aqueous environment of the pore, unlike the wild-type tryptophan.

Gating changes in *I*-W53C

The cysteine substitution mutant *I*-W53C alters the Cd^{2+} and TTX sensitivities of the expressed channel, consistent with its predicted location within the pore of the channel. The unexpected finding is that this substitution also has profound effects on gating. When the α-subunit of the brain or skeletal muscle Na channel is expressed in *Xenopus* oocytes, whole-cell current decay is remarkably slow compared with channels in native tissue (Noda et al., 1989; Trimmer et al., 1989). This functional difference has been attributed to the lack of subsidiary protein components of the channel, possibly the β1 subunit (Krafte et al., 1988; Auld et al., 1988). The cardiac α-subunit similarly expressed decays faster than either the brain or skeletal muscle isoforms, albeit still more slowly than in native tissue (Satin et al., 1992b). *I*-W53C produces a Na channel with faster whole-cell current decay than either the skeletal muscle or cardiac isoforms (Fig. 6 *C*).

At the single-channel level, *I*-W53C exhibits apparent alterations in both activation and inactivation properties. The mutant channel has a brief mean open time that is voltage independent and opens with a short first latency that is less voltage dependent than the wild-type (Fig. 7 *C*). This channel

rarely reopens during a depolarizing epoch, consistent with the idea that it rapidly enters an absorbing inactivated state.

Structural correlates for activation and fast inactivation in Na channels are well described. The cytoplasmic linker between the third and fourth domains of the channel has been shown to be a crucial structural component of fast inactivation. This finding has been confirmed by a variety of approaches, including site-directed antibodies (Vassilev et al., 1988), site-directed mutagenesis (Stühmer et al., 1989; Moorman et al., 1990; Patton et al., 1992; West et al., 1992), and site-specific phosphorylation (West et al., 1991). A popular molecular model of this region of the channel is that of a hinged lid (West et al., 1992) that acts to obstruct current flow through the channel when it is inactivated. The III-IV linker also influences the voltage dependence of activation, particularly when the electrical charge of this region is altered (Moorman et al., 1990; Patton et al., 1992). The principal structural motif involved in activation gating in the Na channel may be the highly charged S4 transmembrane segments (Stühmer et al., 1989). It has been suggested that charge changes in the III-IV linker that affect activation gating do so as a result of interaction with the S4 voltage sensor (Patton et al., 1992) or by alteration of the cytoplasmic surface charge (Cukierman, 1991). A variety of mutations that produce skeletal myopathies are also known to affect Na channel gating (Rüdel et al., 1993). The mutations producing these myotonic diseases occur in various cytoplasmic or transmembrane regions of the channel, but none is predicted to be in the pore. The site of the *I*-W53C mutation is accessible to the external side of the channel, remote from the inactivation gating apparatus, yet it hastens the rate at which the channel gets to an absorbing state. The modeling data help to reconcile the gating effects and the predicted location of this residue in the channel pore (see below); that is, the apparent effects on inactivation gating could be indirect, secondary to changes in activation and deactivation rates produced by the mutation. Residues in the K channel pore have been shown to influence gating (Busch et al., 1991; De Biasi et al., 1992), but this is the first report of such an effect in the Na channel. These data further support the intimate interrelationship of gating and permeation in voltage-gated ion channels.

We have been able to simulate the apparent changes in inactivation by fixing microscopic inactivation rate constants and only permitting changes in activation rate constants relative to the wild-type channel (Fig. 8 and Table 2). The rapid whole-cell current decay of *I*-W53C channels is manifest at the single-channel level as a dramatic reduction in late openings. The model predicts a more rapid deactivation (δ) rate than the wild-type channel, reducing open-state occupancy, and increasing the occupancy of the closed state C_5 from which inactivation is fast (large k_2/k_1) in both mutant and wild-type channels. Thus, most, if not all, of the effects of this mutation on macroscopic inactivation can be explained by changes in microscopic activation and deactivation kinetics.

Molecular fantasy

The *I*-W53C mutation changes both extracellular divalent cation blockade of the Na channel and inward Na^+ conductance compared with the wild-type channel. Multiple effects on both macroscopic and microscopic gating are observed with this mutation compared with the wild-type channel. The location of this residue distant from the proposed inactivation gate argues against a direct interaction of the structural change produced by the mutation and the fast inactivation process. Much more plausible, on the basis of the favored structural models of the Na channel and the modeling results (Fig. 8), is an indirect effect on inactivation gating produced by changes in the activation process. If the relative occupancy of the closed and open states are critical determinants in a non-rate-limiting inactivation process, the apparent changes in inactivation follow directly from the mutation-induced changes in activation kinetics. It is conceivable that the replacement of this aromatic tryptophan in the pore of the channel alters the interaction of the pore of the channel with the voltage sensor. Indeed, the bulky tryptophan residue may serve as a linchpin that slows entry into the open channel conformation.

The work was supported by National Institutes of Health grants HL 50411 (G.F.T.), HL 52307 (E.M.), and T32 HL 07227 (D.W.O.); Medical Research Council, Canada (N.C. and P.H.B.); American Heart Association (AHA), Maryland Affiliate (H.B.N.); AHA-Clinical Scientist Award and Passano Clinician Scientist Award of the Johns Hopkins School of Medicine (J.R. B.); and the Ramon Areces Foundation, Spain (M.T.P.-G.).

REFERENCES

Akabas, M. H., D. A. Stauffer, M. Xu, and A. Karlin. 1992. Acetylcholine receptor channel structure probed in cysteine-substitution mutants. *Science.* 258:307–310.

Aldrich, R. W., D. P. Corey, and C. F. Stevens. 1983. A reinterpretation of mammalian sodium channel gating based on single channel recording. *Nature.* 306:436–441.

Armstrong, C. M. 1971. Interaction of tetraethylammonium ion derivatives with potassium ions of giant axons. *J. Gen. Physiol.* 58:413–437.

Auld, V. J., A. L. Goldin, D. S. Krafte, J. Marshall, J. M. Dunn, W. A. Catterall, H. A. Lester, N. Davidson, and R. J. Dunn. 1988. A rat brain Na^+ channel α-subunit with novel gating properties. *Neuron.* 1:449–461.

Backx, P. H., D. T. Yue, J. H. Lawrence, E. Marban, and G. F. Tomaselli. 1992. Molecular localization of an ion-binding site within the pore of mammalian sodium channels. *Science.* 257:248–251.

Balser, J. R., P. B. Bennett, and D. M. Roden. 1990a. Time-dependent outward current in guinea pig ventricular myocytes: gating kinetics of the delayed rectifier. *J. Gen. Physiol.* 96:835–863.

Balser, J. R., D. M. Roden, and P. B. Bennett. 1990b. Global parameter optimization for cardiac potassium channel gating models. *Biophys. J.* 57:433–444.

Berg, J. M. 1990. Zinc finger domains: hypotheses and current knowledge. *Annu. Rev. Biophys. Biophys. Chem.* 19:405–421.

Blatz, A. L., and K. L. Magleby. 1986. Correcting single channel data for missed events. *Biophys. J.* 49:967–980

Busch, A. E., R. S. Hurst, R. A. North, J. P. Adelman, and M. P. Kavanaugh. 1991. Current inactivation involves a histidine residue in the pore of the rat lymphocyte potassium channel RGK5. *Biochem. Biophys. Res. Commun.* 179:1384–1390.

Cannon S. C., A. McClatchey, and J. F. Gusella. 1993. Modification of the Na^+ current conducted by the rat skeletal muscle α-subunit by coexpression with a human brain β subunit. *Pflügers Arch.* 423:155–157.

Colquhoun, D., and F. S. Sigworth. 1983. Fitting and statistical analysis of single-channel records. *In* Single-Channel Recording. B. Sakmann and E. Neher, editors. Plenum Press, New York. 191–263.

Cukierman, S. 1991. Asymmetric electrostatic effects on the gating of rat brain sodium channels in planar lipid membranes. *Biophys. J.* 60:845–855.

De Biasi, M., H. A. Hartmann, J. A. Drewe, M. Taglialatela, A. M. Brown, and G. E. Kirsch. 1993. Inactivation determined by a single site in K^+ pores. *Pflügers Arch.* 422:354–363.

Demo, S. D., and G. Yellen. 1992. Ion effects on gating of the Ca^{2+}-activated K^+ channel correlate with occupancy of the pore. *Biophys. J.* 61:639–648.

Doyle, D. A., Y. Guo, L. Lustig, J. Satin, R. B. Rogart, and H. A. Fozzard. 1993. Divalent cation competition with [^{3}H]saxitoxin binding to tetrodotoxin-resistant and -sensitive sodium channels. *J. Gen. Physiol.* 101:153–182.

Frelin, C., P. Cognard, P. Vigne, and M. Lazdunski. 1986. Tetrodotoxin-sensitive and tetrodotoxin-resistant Na^+ channels differ in their sensitivity to Cd^{2+} and Zn^{2+}. *Eur. J. Pharmacol.* 122:245–250.

Guy, H. R., and P. Seetharamulu. 1986. Molecular model of the action potential sodium channel. *Proc. Natl. Acad. Sci. USA.* 83:508–512.

Hamill, O. P., A. Marty, E. Neher, B. Sakmann, and F. J. Sigworth 1981. Improved patch-clamp technique for high-resolution current recording from cells and cell-free membrane patches. *Pflügers Arch.* 391:85–100.

Hille, B. 1992. Ionic Channels of Excitable Membranes. Sinauer Associates, Sunderland, MA.

Hindmarsh, A. C. 1983. Odepack, a systematized collection of ode solvers. *In* Scientific Computing. R. S. Stepleman, editor. North-Holland Publishing, Amsterdam. 55–64.

Hodgkin, A. L., and Huxley A. F. 1952. A quantitative description of membrane current and its application to conduction and excitability in nerve. *J. Physiol.* 117:500–544.

Holloway, S. F., V. F. Salgado, C. Wu, and T. Narahashi. 1989. Kinetic properties of single sodium channels modified by fenvalerate in mouse neuroblastoma cells. *Pflügers Arch.* 414:613–621.

Hoshi, T., W. N. Zagotta, and R. W. Aldrich. 1990. Biophysical and molecular mechanisms of *Shaker* potassium channel inactivation. *Science.* 250:533–538.

Hoshi, T., W. N. Zagotta, and R. W. Aldrich 1991. Two types of inactivation in *Shaker* K^+ channels: effects of alterations in the carboxy-terminal region. *Neuron.* 7:547–556.

Isacoff, E. Y., Y. N. Jan, L. Y. Jan. 1991. Putative receptor for the cytoplasmic inactivation gate in the *Shaker* K^+ channel. *Nature.* 353:86–90.

Isom, L. L., K. S. De Jongh, D. E. Patton, B. F. X. Reber, J. Offord, H. Charbonneau, K. Walsh, A. L. Goldin, and W. A. Catterall. 1992. Primary structure and functional expression of the β_1 subunit of the rat brain sodium channel. *Science.* 256:839–842.

Kirsch, G. E., J. A. Drewe, H. A. Hartmann, M. Tagialatela, M. De Biasi, A. M. Brown, and R. Joho. 1992. Differences between the deep pores of K^+ channels determined by an interacting pair of nonpolar amino acids. *Neuron.* 8:499–505.

Krafte, D. S., Snutch T. P., J. P. Leonard, N. Davidson, H. A. Lester. 1988. Evidence for the involvement of more than one mRNA species in controlling the inactivation process of rat and rabbit brain Na channels expressed in *Xenopus* oocytes. *J. Neurosci.* 8:2859–2868.

Kreig, P. A., and D. A. Melton. Functional messenger RNAs are produced by SP6 in vitro transcription of cloned cDNAs. *Nucleic Acids Res. 1984.* 12:7057–7070.

Kunkel, T. A. 1985. Rapid, and efficient site-specific mutagenesis with phenotypic selection. *Proc. Natl. Acad. Sci. USA.* 82:488–492.

Kuo, C.-C., and B. P. Bean. 1994. Na^+ channels must deactivate to recover from inactivation. *Neuron.* 12:819–829.

Kürz, L. L., H.-J. Zhang, R. D. Zühlke, and R. H. Joho. 1994. Probing the mouth of a K^+ channel by a sulfhydryl-reagent after cysteine substitution mutagenesis. *Biophys. J.* 66:A24.

Lipkind, G., and H. A. Fozzard. 1994. A structural model of the tetrodotoxin and saxitoxin binding site of the Na^+ channel. *Biophys. J.* 66:1–13.

Matteson, D. R., and R. P. Swenson. 1986. External monovalent cations that impede the closing of K^+ channels. *J. Gen. Physiol.* 87:795–816.

McCormack, K., M. A. Tanouye, L. E. Iverson, J.-W. Lin, M. Ramaswami, T. McCormack, J. T. Campanelli, M. K. Mathew, and B. Rudy. 1991. A role for hydrophobic residues in the voltage-dependent gating of Shaker K^+ channels. *Proc. Natl. Acad. Sci. USA.* 88:2931–2935.

Miller, C. R., R. Latorre, and I. Reisin. 1987. Coupling of voltage-dependent gating and Ba^{2+} block in high conductance Ca^{2+}-activated K channel. *J. Gen. Physiol.* 90:427–449.

Moorman, J. R., G. E. Kirsch, A. M. J. VanDongen, R. H. Joho, and A. M. Brown. 1990. Fast and slow gating of sodium channels encoded by a single mRNA. *Neuron.* 4:243–252.

Nelder, J. A., and R. Mead. 1965. A simplex method for function minimization. *Computer J.* 7:308–313.

Noda, M., T. Ikeda, H. Suzuki, H. Takeshima, H. Takahashi, M. Kuno, and S. Numa. 1986. Expression of functional sodium channels from cDNA. *Nature.* 322:826–828.

Noda, M., H. Suzuki, S. Numa, and W. Stühmer. 1989. A single point mutation confers tetrodotoxin, and saxitoxin insensitivity on the sodium channel II. *FEBS Lett.* 259:213–216.

Pardo L. A., S. H. Heinemann, H. Terlau, U. Ludewig, C. Lorra, O. Pongs, and W. Stühmer. 1992. Extracellular K^+ specifically modulates a rat brain K^+ channel. *Proc. Natl. Acad. Sci. USA.* 89:2466–2470.

Patton, D. E., J. W. West, T. Scheuer, Y. Wang, A. L. Goldin, and W. A. Catterall. 1992. Amino acid residues required for fast Na^+-channel inactivation: charge neutralizations and deletions in the III-IV linker. *Proc. Natl. Acad. Sci. USA.* 89:10905–10909.

Petzold, L. R. 1983. Automatic selection of methods for solving stiff and nonstiff systems of ordinary differential equations. *Soc. Ind. Appl. Math. J. Sci. Stat. Comput.* 4:136–148.

Pusch, M., M. Noda, W. Stühmer, S. Numa, and F. Conti. 1991. Single point mutations of the sodium channel drastically reduce the pore permeability without preventing its gating. *Eur. Biophys. J.* 20:127–133.

Rogart, R. B., L. L. Cribbs, L. K. Muglia, D. D. Kephart, and M. W. Kaiser. 1989. Molecular cloning of a putative tetrodotoxin-resistant rat heart Na^+ channel isoform. *Proc. Natl. Acad. Sci. USA.* 86:8170–8174.

Rüdel, R., K. Ricker, and F. Lehmann-Horn. 1993. Genotype-phenotype correlations in human skeletal muscle sodium channel diseases. *Arch. Neurol.* 50:1241–1248.

Sanger, F., S. Nicklen, and A. R. Coulson. 1977. DNA sequencing with chain-terminating inhibitors. *Proc. Natl. Acad. Sci. USA.* 74:5463–5467.

Satin, J., J. W. Kyle, M. Chen, P. Bell, L. Cribbs, H. A. Fozzard, and R. B. Rogart. 1992a. A mutant of TTX-resistant cardiac sodium channels with TTX-sensitive properties. *Science.* 256:1202–1205.

Satin, J., J. W. Kyle, M. Chen, R. B. Rogart, and H. A. Fozzard. 1992b. The cloned cardiac Na channel α-subunit expressed in *Xenopus* oocytes show gating and blocking properties of native channels. *J. Membr. Biol.* 130: 11–22.

Scheuer, T., V. Auld, S. Boyd, J. Offord, R. Dunn, and W. A. Catterall. 1990. Functional properties of rat brain sodium channels expressed in a somatic cell line. *Science.* 247:854–858.

Schild, L., and E. Moczydlowski. 1991. Competitive binding interaction between Zn^{2+} and saxitoxin in cardiac Na^+ channels: evidence for a sulfhydryl group in the Zn^{2+}/saxitoxin binding site. *Biophys. J.* 59: 523–537.

Stühmer, W., F. Conti, H. Suzuki, X. Wang, M. Noda, N. Yahagi, H. Kubo, and S. Numa. 1989. Structural parts involved in activation and inactivation of the sodium channel. *Nature.* 339:597–603.

Terlau, H., S. H. Heinemann, W. Stühmer, M. Pusch, F. Conti, K. Imoto, and S. Numa. 1991. Mapping the site of block by tetrodotoxin and saxitoxin of sodium channel II. *FEBS Lett.* 293:93–96.

Tomaselli, G. F., P. H. Backx, and E. Marban. 1993a. Molecular basis of permeation in voltage-gated ion channels. *Circ. Res.* 72:491–496.

Tomaselli, G. F., K. A. Kluge, M. T. Peréz-García, and E. Marban. 1994. Serial cysteine substitutions reveal functional asymmetries in the pore of the sodium channel. *Circulation.* 90:I197a.

Tomaselli, G. F., H. B. Nuss, K. Kluge, J. H. Lawrence, P. H. Backx, and

E. Marban. 1993b. A mutation in the pore of the Na^+ channel alters inactivation. *Circulation*. 88:I987a.

Tomaselli, G. F., H. B. Nuss, J. H. Lawrence, P. H. Backx, and E. Marban. 1993c. A cysteine substitution in the P-region of the skeletal muscle sodium channel alters sensitivity to tetrodotoxin and divalent cations. *Biophys. J.* 64:88a.

Trimmer, J. S., S. S. Cooperman, S. A. Tomiko, J. Zhou, S. M. Crean, M. B. Boyle, R. G. Kallen, Z. Sheng, R. L. Barchi, F. J. Sigworth, R. H. Goodman, W. S. Agnew, and G. Mandel. 1989. Primary structure and functional expression of a mammalian skeletal muscle sodium channel. *Neuron*. 3:33–49.

Vassilev, P. M., T. Scheuer, and W. A. Catterall. 1988. Identification of an intracellular peptide segment involved in sodium channel inactivation. *Science*. 241:1658–1661.

West, J. W., R. Numann, B. J. Murphy, T. Scheuer, and W. A. Catterall. 1991. A phosphorylation site in the sodium channel required for modulation by protein kinase C. *Science*. 254:866–868.

West, J. W., D. E. Patton, T. Scheuer, Y. Wang, A. L. Goldin, and W. A. Catterall. 1992. A cluster of hydrophobic amino acid residues required for fast Na^+-channel inactivation. *Proc. Natl. Acad. Sci. USA*. 89:10910–10914.

Woodhull, A. M. 1973. Ionic blockage of sodium channels in nerve. *J. Gen. Physiol.* 61:687–708.

Yellen, G., D. Sodickson, T.-Y. Chen, and M. E. Jurman. 1994. An engineered cysteine in the external mouth of a K^+ channel allows inactivation to be modulated by metal binding. *Biophys. J.* 66:1068–1075.

Yue, D. T., J. H. Lawrence, E. Marban. 1989. Two molecular transitions influence cardiac sodium channel gating. *Science*. 244:349–352.

Zhou, J., J. F. Potts, J. S. Trimmer, W. S. Agnew, and F. J. Sigworth. 1991. Multiple gating modes and the effect of modulating factors on the μ1 sodium channel. *Neuron*. 7:775–785.